Lithium ions display weak interaction with amyloid-beta (Aβ) peptides and have minor effects on their aggregation

Elina Berntsson[1,2], Suman Paul[1], Faraz Vosough[1], Sabrina B. Sholts[3], Jüri Jarvet[1,4], Per M. Roos[5,6], Andreas Barth[1], Astrid Gräslund[1], Sebastian K. T. S. Wärmländer[1,*]

[1] Department of Biochemistry and Biophysics, Stockholm University, Sweden.
[2] Department of Chemistry and Biotechnology, Tallinn University of Technology, Estonia;
[3] Department of Anthropology, National Museum of Natural History, Smithsonian Institution, Washington, DC, USA.
[4] The National Institute of Chemical Physics and Biophysics, Tallinn, Estonia.
[5] Institute of Environmental Medicine, Karolinska Institutet, Stockholm, Sweden.
[6] Department of Clinical Physiology, Capio St. Göran Hospital, Stockholm, Sweden.
***** Correspondence: seb@dbb.su.se; Tel.: +46 8 162444

Abstract: Alzheimer's disease (AD) is an incurable disease and the main cause of age-related dementia worldwide, despite decades of research. Treatment of AD with lithium (Li) has showed promising results, but the underlying mechanism is unclear. The pathological hallmark of AD brains is deposition of amyloid plaques, consisting mainly of amyloid-β (Aβ) peptides aggregated into amyloid fibrils. The plaques contain also metal ions of e.g. Cu, Fe, and Zn, and such ions are known to interact with Aβ peptides and modulate their aggregation and toxicity. The interactions between Aβ peptides and Li^+ ions have however not been well investigated. Here, we use a range of biophysical techniques to characterize *in vitro* interactions between Aβ peptides and Li^+ ions. We show that Li^+ ions display weak and non-specific interactions with Aβ peptides, and have minor effects on Aβ aggregation. These results indicate that possible beneficial effects of Li on AD pathology are not likely caused by direct interactions between Aβ peptides and Li^+ ions.

Key Words: Alzheimer's disease; protein aggregation; Metal-protein binding; Neurodegeneration; Pharmaceutics

Running Title: Li^+ ions have minor effects on Aβ aggregation

INTRODUCTION

Alzheimer's disease (AD) is still an incurable disease and the main cause of age-related dementia worldwide (Querfurth & LaFerla, 2010; Prince *et al.*, 2015; Frozza *et al.*, 2018), despite decades of research on putative drugs (Luo *et al.*, 2013; Wärmländer *et al.*, 2013; Decker & Munoz-Torrero, 2016; Kisby *et al.*, 2019). In addition to signs of neuroinflammation and oxidative stress (Agostinho *et al.*, 2010; Al-Hilaly *et al.*, 2013; Wang *et al.*, 2014; Heppner *et al.*, 2015; Regen *et al.*, 2017), AD brains display characteristic lesions in the form of intracellular neurofibrillary tangles, consisting of aggregated hyperphosphorylated tau proteins (Goedert, 2018; Gibbons *et al.*, 2019), and extracellular amyloid plaques, consisting mainly of insoluble fibrillar aggregates of amyloid-β (Aβ) peptides (Glenner & Wong, 1984; Querfurth & LaFerla, 2010). These Aβ fibrils and plaques are the end-product of an aggregation process (Querfurth & LaFerla, 2010; Luo *et al.*, 2016; Selkoe & Hardy, 2016) that involves extra- and/or intracellular formation of intermediate, soluble, and likely neurotoxic Aβ oligomers (Luo *et al.*, 2014; Selkoe & Hardy, 2016; Sengupta *et al.*, 2016; Lee *et al.*, 2017) that can spread from neuron to neuron via exosomes (Nath *et al.*, 2012; Sardar Sinha *et al.*, 2018).

The Aβ peptides comprise 37-43 residues and are intrinsically disordered in aqueous solution. They have limited solubility in water due to the hydrophobicity of the central and C-terminal Aβ segments, which may fold into a hairpin conformation upon aggregation (Abelein *et al.*, 2014; Baronio *et al.*, 2019). The charged N-terminal segment is hydrophilic and readily interacts with cationic molecules and metal ions (Luo *et al.*, 2013; Luo *et al.*, 2014; Tiiman *et al.*, 2016; Wallin *et al.*, 2016; Wallin *et al.*, 2017; Owen *et al.*, 2019; Wallin *et al.*, 2020), while the hydrophobic C-terminal segment can interact with membranes where Aβ may exert its toxicity (Österlund *et al.*, 2018; Wärmländer *et al.*, 2019). The interactions between Aβ and metal ions are of particular interest (Duce *et al.*, 2011; Wärmländer *et al.*,

2013; Mital *et al.*, 2015; Wärmländer *et al.*, 2019; Wallin *et al.*, 2020), as altered metal concentrations indicative of metal dyshomeostasis are a prominent feature in the brains and fluids of AD patients (Wang *et al.*, 2015; Szabo *et al.*, 2016), and because AD plaques contain elevated amounts of metal ions of e.g. Cu, Fe, and Zn (Beauchemin & Kisilevsky, 1998; Lovell *et al.*, 1998; Miller *et al.*, 2006).

Interestingly, although the role of metal ions in AD pathogenesis remains debated (Duce *et al.*, 2011; Modgil *et al.*, 2014; Chin-Chan *et al.*, 2015; Mital *et al.*, 2015; Adlard & Bush, 2018; Huat *et al.*, 2019; Wärmländer *et al.*, 2019), monovalent ions of the alkali metal lithium [i.e., Li^+ ions] may provide beneficial effects to patients with neurodegenerative disorders such as amyotrophic lateral sclerosis (ALS) (Fornai *et al.*, 2008; Morrison *et al.*, 2013) or AD (Engel *et al.*, 2008; Mauer *et al.*, 2014; Sutherland & Duthie, 2015; Decker & Munoz-Torrero, 2016; Donix & Bauer, 2016; Morris & Berk, 2016; Kerr *et al.*, 2018; Hampel *et al.*, 2019; Kisby *et al.*, 2019; Priebe & Kanzawa, 2020). Lithium salts are commonly used in psychiatric medication, even though it is not understood how the Li^+ ions affect the molecular mechanisms underlying the psychiatric disorders (Dell'Osso *et al.*, 2016). Unlike other pharmaceuticals, Li^+ is widely non-selective in its biochemical effects, possibly due to its general propensity to inhibit the many enzymes that have magnesium as a cofactor (Ge & Jakobsson, 2018).

Cell and animal studies have provided clues regarding how Li^+ ions may affect the AD disease pathology (Nery *et al.*, 2014; Sofola-Adesakin *et al.*, 2014; Zhao *et al.*, 2014; Budni *et al.*, 2017; Habib *et al.*, 2017; Cardillo *et al.*, 2018; Kerr *et al.*, 2018; Habib *et al.*, 2019; Rocha *et al.*, 2020; Wilson *et al.*, 2020). Due to its ability to down-regulate translation, Li^+ caused a reduction in protein synthesis and thus $A\beta_{42}$ levels in an adult-onset Drosophila model of AD (Sofola-Adesakin *et al.*, 2014). Li^+ reduces Aβ production by affecting the processing/cleavage of the amyloid-β precursor protein (AβPP) in cells and mice, presumably

by down-regulating the levels of phosphorylated APP. A main target of Li^+ is the glycogen synthase kinase 3-beta (GSK-3β) (Ryves & Harwood, 2001) which is implicated in AD pathogenesis (Caccamo *et al.*, 2007; Forlenza *et al.*, 2014). In AβPP-transgenic mice, reduced activation of the GSK-3β enzyme was associated with decreased levels of APP phosphorylation that resulted in decreased Aβ production (Rockenstein *et al.*, 2007). One study on mice with traumatic brain injury reported that Li^+-treatment improved spatial learning and reduced Aβ production, possibly by reducing the levels of both AβPP and the AβPP-cleaving enzyme BACE1 (Yu *et al.*, 2012). More recent mice studies have reported that treatment with Li^+ ions improved Aβ clearance from the brain (Pan *et al.*, 2018), reduced oxidative stress levels (Xiang *et al.*, 2020), improved spatial memory (Habib *et al.*, 2019), and reduced the amounts of Aβ plaques and phosphorylated tau while also improving spatial memory (Liu *et al.*, 2020).

Only a few studies have however investigated how Li^+ ions could affect the molecular events that appear to underlie AD pathology, such as Aβ aggregation. One study showed that increased ionic strength, i.e. 150 mM of NaF, NaCl, or LiCl, significantly accelerated the kinetics of Aβ amyloid formation, by promoting surface-catalyzed secondary nucleation reactions (Abelein *et al.*, 2016). Another recent study used molecular dynamics simulations to find small but distinct differences in how the three monovalent Li^+, N^+, and K^+ ions interact with Aβ oligomers (Huraskin & Horn, 2019). The therapeutic effect of Li^+ on Aβ plaque quality and toxicity has been reported in mice, where Li^+ treatment before pathology onset induced smaller plaques with higher Aβ compaction, reduced oligomeric-positive halo, and attenuated capacity to induce neuronal damage (Trujillo-Estrada *et al.*, 2013). One hypothesis is that these neuroprotective effects of Li^+ could be mediated by modifications of the plaque toxicity through the astrocytic release of heat shock proteins (Trujillo-Estrada *et al.*, 2013).

Here, we use a range of biophysical techniques to characterize the *in vitro* interactions between Li^+ ions and Aβ peptides, and how such interactions affect the Aβ amyloid aggregation processes and fibril formation.

MATERIALS AND METHODS

Sample preparation

Recombinant $A\beta_{40}$ peptides were purchased from AlexoTech AB (Umeå, Sweden) in either unlabeled or uniformly ^{15}N-labeled form. The lyophilized peptides were stored at -80 °C. Samples were dissolved to monomeric form immediately before each measurement. The peptides were first dissolved in 10 mM NaOH, and then sonicated in an ice-bath to avoid having pre-formed aggregates in the sample solutions. Next, the samples were diluted in 20 mM buffer of either sodium phosphate or MES (2-[N-morpholino]ethanesulfonic acid). All preparation steps were performed on a bed of ice, and the peptide concentration was determined by weight. LiCl salt was purchased from Merck & Co. Inc. (USA), and MES hydrate was purchased from Sigma-Aldrich (USA).

Synthetic $A\beta_{42}$ peptides were purchased from JPT Peptide Technologies (Germany) and used to prepare monomeric solutions via size exclusion chromatography. 1 mg of lyophilized $A\beta_{42}$ powder was dissolved in 250 mL DMSO. A Sephadex G-250 HiTrap desalting column (GE Healthcare, Uppsala) was equilibrated with 5 mM NaOH solution (pH=12.3), and washed with 10-15 mL of 5 mM NaOD, pD=12.7 (Glasoe & Long, 1960) solution. The peptide solution in DMSO was applied to the column, followed by injection of 1.25 mL of 5 mM NaOD. Collection of peptide fractions in 5 mM NaOD on ice was started at a 1 mg/mL flow rate. Ten fractions of 1 mL volumes were collected in 1.5 mL Eppendorf tubes. The absorbance for each fraction at 280 nm was measured with a NanoDrop instrument (Eppendorf, Germany), and peptide concentrations were determined using a molar extinction

coefficient of 1280 $M^{-1}cm^{-1}$ for the single Tyr in $A\beta_{42}$ (Edelhoch, 1967). The peptide fractions were flash-frozen in liquid nitrogen, covered with argon gas on top in 1.5 mL Eppendorf tubes, and stored at -80°C until used. Sodium dodecyl sulfate (SDS)-stabilized $A\beta_{42}$ oligomers of two well-defined sizes (approximately tetramers and dodecamers) were prepared according to a previously published protocol (Barghorn *et al.*, 2005), but in D_2O, at 4-fold lower peptide concentration and without the original dilution step (Vosough & Barth, manuscript). The reaction mixtures (100 µM $A\beta_{42}$ in PBS and containing 0.05 % or 0.2% SDS) were incubated together with 0-10 mM LiCl at 37 °C for 24 hours, and then flash-frozen in liquid nitrogen and stored at -20°C for later analysis.

Thioflavin T kinetics

A FLUOstar Omega microplate reader (BMG LABTECH, Germany) was used to monitor the effect of Li^+ ions on Aβ aggregation kinetics, 20 µM monomeric $A\beta_{40}$ peptides were incubated in 20 mM MES buffer, pH 7.35, together with different concentrations of LiCl (0, 20 µM, 200 µM, 2000 µM) and 50 µM Thioflavin T (ThT). ThT is a fluorescent benzothiazole dye, and its fluorescence intensity increases when bound to amyloid aggregates (Gade Malmos *et al.*, 2017). Samples were placed in a 96-well plate where the sample volume in each well was 100 µL, four replicates per Li^+ concentration were measured, the temperature was +37 °C, excitation of the ThT dye was at 440 nm, the ThT fluorescence emission at 480 nm was measured every five minutes, each five-minute cycle involved 140 seconds of shaking at 200 rpm, the samples were incubated for a total of 15 hours, and the assay was repeated three times. To derive parameters for the aggregation kinetics, the ThT fluorescence curves were fitted to the sigmoidal equation 1:

$$F(t) = F_0 + m_0 \cdot t + \frac{F_\infty + m_\infty \cdot t}{1 + exp - [(t - t_{1/2})/\tau]} \qquad \text{(Eq. 1)}$$

where F_0 and F_∞ are the intercepts of the initial and final fluorescence intensity baselines, m_0 and m_∞ are the slopes of the initial and final baselines, $t_{½}$ is the time needed to reach halfway through the elongation phase (i.e., aggregation half-time), and τ is the elongation time constant (Gade Malmos *et al.*, 2017). The apparent maximum rate constant, r_{max}, for the growth of fibrils is given by $1/\tau$.

Tyrosine fluorescence quenching

The binding affinity between $A\beta_{40}$ peptides and Li^+ ions was evaluated from Cu^{2+}/ Li^+ binding competition experiments (Wallin *et al.*, 2020). The affinity of the Cu^{2+}·$A\beta_{40}$ complex was measured *via* the quenching effect of Cu^{2+} ions on the intrinsic fluorescence of Y10, which is the only fluorophore in native Aβ peptides. The fluorescence emission intensity at 305 nm (excitation wavelength 276 nm) was recorded at 20 °C using a Jobin Yvon Horiba Fluorolog 3 fluorescence spectrophotometer (Longjumeau, France). The titrations were carried out by consecutive additions of 0.8 – 3.2 µL aliquots of either 2, 10, or 50 mM stock solutions of $CuCl_2$ to 800 µL of 10 µM $A\beta_{40}$ in 20 mM MES buffer, pH 7.35, in a quartz cuvette with 4 mm path length. After each addition of $CuCl_2$ the solution was stirred for 30 seconds before recording fluorescence emission spectra. Copper titrations were conducted for $A\beta_{40}$ samples both in the absence and the presence of 1 mM LiCl. The dissociation constant of the Cu^{2+}·$A\beta_{40}$ complex was determined by fitting the Cu^{2+} titration data to equation 2:

$$I = I_0 + \frac{I_\infty - I_0}{2\cdot[A\beta]} \cdot \left((K_D + [Cu] + [A\beta]) - \sqrt{(K_D + [Cu] + [A\beta])^2 - 4\cdot[Cu]\cdot[A\beta]} \right) - k\cdot[Cu]$$

(Eq. 2)

where I_0 is the initial fluorescence intensity without Cu^{2+} ions, I_∞ is the steady-state (saturated) intensity at the end of the titration series, [Aβ] is the peptide concentration, [Cu] is the concentration of added Cu^{2+} ions, K_D is the dissociation constant of the Cu^{2+}·$A\beta_{40}$ complex, and k is a constant accounting for the concentration-dependent quenching effect induced by free (non-bound) Cu^{2+} ions that may collide with the Y10 residue (Lindgren *et al.*, 2013). This model assumes a single binding site. As no corrections for buffer conditions are made, i.e. in terms of possible interactions between the metal ions and the buffer, the calculated dissociation constant should be considered to be apparent.

Atomic force microscopy imaging

Samples of 20 µM $A\beta_{40}$ in 5 mM MES buffer (total volume 100 µL, pH 7.35) with either 0, 20 µM, 200 µM or 2 mM LiCl were put in small Eppendorf tubes and incubated for 72 hours at 37 ^oC under continuous shaking at 300 rpm. A droplet (1 µL) of incubated solution was then placed on a fresh silicon wafer (Siegert Wafer GmbH, Germany) and left to dry for 2 minutes. Next, 10 uL of Milli-Q H_2O was carefully added to the semi-dried sample droplet and soaked immediately with a lint-free wipe, to remove excess salts in a mild manner. The wafer was left to dry in a covered container to protect it from dust, and atomic force microscopy (AFM) images were recorded on the same day. A neaSNOM scattering-type near-field optical instrument (Neaspec GmbH, Germany) was used to collect the AFM images under tapping mode (Ω: 280 kHz, tapping amplitude 50-55 nm) using Pt/Ir-coated monolithic ARROW-NCPt Si tips (NanoAndMore GmbH, Germany) with tip radius <10 nm. Images were acquired on 2.5 x 2.5 µm scan-areas (200 x 200-pixel size) under optimal scan-speed (i.e., 2.5 ms/pixel). The recorded images were minimally processed using the Gwyddion software where a basic plane leveling was performed (Nečas & Klapetek, 2012).

Nuclear magnetic resonance spectroscopy

An Avance 700 MHz nuclear magnetic resonance (NMR) spectrometer (Bruker Inc., USA) equipped with a cryoprobe was used to investigate possible interactions between Li^+ ions and monomeric $A\beta_{40}$ peptides at the atomic level. 2D ^{1}H-^{15}N-HSQC spectra of 92.4 µM monomeric ^{15}N-labeled $A\beta_{40}$ peptides were recorded at 5 °C with 90/10 H_2O/D_2O, either in 20 mM MES buffer at pH 7.35 or in 1x PBS buffer (137 mM NaCl, 2.7 mM KCl, and 10 mM phosphate pH 7.4), before and after additions with LiCl. Diffusion measurements were performed on a sample of 55 µM unlabeled monomeric $A\beta_{40}$ peptide in 20 mM sodium phosphate buffer, 100 % D_2O, pD 7.5, at 5 °C, before and after additions with LiCl dissolved in D_2O. The diffusion experiments employed pulsed field gradients (PFG:s) according to previously described methods (Danielsson *et al.*, 2002), and methyl group signals between 0.7-0.4 ppm were integrated, evaluated, and corrected for the viscosity of D_2O at 5 °C (Cho *et al.*, 1999). All NMR data was processed with the Topspin version 3.6.2 software, and the HSQC crosspeak assignment for $A\beta_{40}$ in buffer is known from previous studies (Danielsson *et al.*, 2006).

Circular dichroism spectroscopy

Circular dichroism (CD) spectra of 20 µM $A\beta_{40}$ peptides in 20 mM sodium phosphate buffer, pH 7.35, were recorded at 20 °C using a Chirascan CD spectrometer (Applied Photophysics, UK) and a quartz cuvette with an optical path length of 2 mm. Measurements were done between 190 − 250 nm, with a step size of 1 nm and a sampling time of 4 s per data point. First, a spectrum was recorded for $A\beta_{40}$ alone. Next, micelles of 50 mM SDS were added to create a membrane-mimicking environment. Finally, LiCl was titrated to the sample in steps up to a concentration of 512 µM.

Blue native polyacrylamide gel electrophoresis

Homogeneous solutions of 100 µM $A\beta_{42}$ oligomers prepared in presence and absence of 0 – 10 mM Li^+ ions were analyzed with blue native polyacrylamide gel electrophoresis (BN-PAGE) using the Invitrogen system. 4-16% Bis-Tris Novex gels (ThermoFisher Scientific, USA) were loaded with 10 µL of $A\beta_{42}$ oligomer samples alongside the Amersham High Molecular Weight calibration kit for native electrophoresis (GE Healthcare, USA). The gels were run at 4 °C using the electrophoresis system according to the Invitrogen instructions (ThermoFisher Scientific, USA), and then stained using the Pierce Silver Staining kit according to the instructions (ThermoFisher Scientific, USA).

Infrared spectroscopy

Fourier-transformed infrared (FTIR) spectra of $A\beta_{42}$ oligomers were recorded in transmission mode on a Tensor 37 FTIR spectrometer (Bruker Optics, Germany) equipped with a sample shutter and a liquid nitrogen-cooled MCT detector. The unit was continuously purged with dry air during the measurements. 8-10 µL of the 80 µM $A\beta_{42}$ oligomer samples, containing 0 – 10 mM LiCl, were put between two flat CaF_2 discs separated by a 50 µm plastic spacer covered with vacuum grease at the periphery. The assembled discs were mounted in a holder inside the instrument's sample chamber. The samples were allowed to sit for at least 15 minutes after closing the chamber lid, to avoid interference from CO_2 and H_2O vapor. FTIR spectra were recorded at room temperature in the 1900-800 cm^{-1} range, with 300 scans for both background and sample spectra, using a 6 mm aperture and a resolution of 2 cm^{-1}. The light intensities above 2200 cm^{-1} and below 1500 cm^{-1} were blocked with respectively a germanium filter and a cellulose membrane (Baldassarre & Barth, 2014). The spectra were analyzed and plotted with the OPUS 5.5 software, and second derivatives were calculated with a 17 cm^{-1} smoothing range.

RESULTS

ThT fluorescence: influence of Li^+ ions on $A\beta_{40}$ aggregation

The fluorescence intensity of the amyloid-marker molecule ThT was measured when 20 μM $A\beta_{40}$ samples were incubated for 15 hours together with different concentrations of LiCl (Fig. 1). Fitting Eq. 1 to the ThT fluorescence curves yielded the kinetic parameters $t_{1/2}$ (aggregation half-time) and r_{max} (maximum aggregation rate) (Fig. 1; Table 1). For 20 μM $A\beta_{40}$ alone, the aggregation half-time is approximately 3.7 hours under the experimental conditions used, and the maximum aggregation rate is 0.5 $hours^{-1}$ (Table 1). These kinetic parameters are not much affected by addition of LiCl in 1:1 or 10:1 Li^+:Aβ ratios. At the Li^+:Aβ ratio of 100:1, the r_{max} value remains largely unaffected while the aggregation half-time is increased to almost 5 hours (Fig 1; Table 1). The observation that a Li^+:Aβ ratio of 100:1 is required to shift the ThT curve clearly shows that Li^+ ions do not have a strong effect on the $A\beta_{40}$ aggregation kinetics.

AFM imaging: effects of Li^+ ions on the morphology of $A\beta_{40}$ aggregates

AFM images (Fig. 2) were recorded for the aggregation products of 20 μM $A\beta_{40}$ peptide, incubated for three days without or with LiCl. The control sample without Li^+ displays long (> 2 μm) amyloid fibrils that are around 6 nm thick, together with small (< 2 nm) aggregate particles that may be protofibrils (Fig. 2A). The distribution and sizes of these aggregates are rather typical for $A\beta_{40}$ aggregates formed *in vitro* (Luo *et al.*, 2014). The $A\beta_{40}$ samples incubated in the presence of different concentrations of Li^+ ions display amyloid fibrils of similar size and shape, although these fibrils are more densely packed and they appear to be more numerous (Figs. 1B, 1C, 1D). Compared to the control sample, there are fewer small (< 2 nm) aggregate particles in the samples incubated together with Li^+ ions in 10:1 and 100:1

Li^+:Aβ ratios. This suggests that Li^+ ions may induce some differences in the $Aβ_{40}$ aggregation process.

NMR spectroscopy: interactions between Li^+ ions and $Aβ_{40}$ monomers

High-resolution liquid phase NMR experiments were conducted to investigate if residue-specific molecular interactions could be observed between Li^+ ions and monomeric $Aβ_{40}$ peptides. 2D ^{1}H-^{15}N-HSQC spectra showing the amide crosspeak region for 92.4 μM monomeric ^{15}N-labeled $Aβ_{40}$ peptides are presented in Fig. 3A, before and after addition of LiCl in 1:1, 1:10, and 1:100 Aβ:Li^+ ratios in 20 mM MES buffer, 7.35. Addition of Li^+ ions induces loss of signal intensity mainly for amide crosspeaks corresponding to residues in the N-terminal half of the peptide, indicating selective Li^+ interactions in this region (Fig. 3B). The effects are clearly concentration-dependent. Because Li^+ ions are not paramagnetic, this loss of signal intensity is arguably caused by chemical exchange related to structural rearrangements induced by the Li^+ ions. As no chemical shift changes are observed for the crosspeak position (Fig. 3A), these Li^+-induced secondary structures appear to be short-lived. Figs. 3C and 3D show the results of similar experiments carried out in 1x PBS buffer, i.e. 137 mM NaCl, 2.7 mM KCl, and 10 mM phosphate pH 7.4. Here, the Li^+ ions induce virtually no changes in the crosspeak intensities, showing that the weak Li^+/$Aβ_{40}$ interactions observed in pure MES buffer (Figs. 3A,B) disappear when the buffer and ionic strength correspond to physiological conditions.

Diffusion measurements were carried out for 55 μM $Aβ_{40}$ peptides in D_2O, before and after addition of LiCl in 1:1, 20:1, and 100:1 Li^+:Aβ ratios. Addition of 1:1 Li^+ produces an increase in the $Aβ_{40}$ diffusion rate by around 4%, i.e. from $5.97 \cdot 10^{-11}$ m^2/s to $6.23 \cdot 10^{-11}$ m^2/s (Figs. 4A and 4B). This somewhat faster diffusion is likely caused by the $Aβ_{40}$ peptide adopting a slightly more compact structure in the presence of Li^+ ions, an effect similar to

that previously reported for zinc ions (Abelein *et al.*, 2015). Addition of even higher Li^+ concentrations – 20 and 100 times the $A\beta_{40}$ concentration – produces diffusion rates that are similar but a little bit lower than the diffusion rate measured for 1:1 Li^+:$A\beta_{40}$ ratio, i.e. respectively $6.19 \cdot 10^{-11}$ m^2/s and $6.15 \cdot 10^{-11}$ m^2/s (Figs. 4C and 4D), indicating that the effect of Li^+ on the $A\beta_{40}$ secondary structure and diffusion has been saturated.

Fluorescence spectroscopy: Li^+ binding affinity to the $A\beta_{40}$ monomer

Binding affinities for metal ions to Aβ peptides can often be measured *via* the quenching effect on the intrinsic fluorescence of Y10, the only fluorophore in native Aβ peptides. However, not all metal ions interfere with tyrosine fluorescence, and initial experiments showed that addition of Li^+ ions does not affect the $A\beta_{40}$ fluorescence. The binding affinity of Li^+ ions to $A\beta_{40}$ was therefore evaluated from binding competition experiments with Cu^{2+} ions (Danielsson *et al.*, 2007; Wallin *et al.*, 2020), which induce much stronger tyrosine fluorescence quenching when bound to the peptide than when free in the solution (Lindgren *et al.*, 2013). Fig. 5 shows the results of titrating $CuCl_2$ to $A\beta_{40}$, both in the absence (red circles) and in the presence (blue triangles) of 1 mM LiCl.

Three titrations were carried out for each condition, producing apparent K_D values for the Cu^{2+}·$A\beta_{40}$ complex of respectively 3.1 µM, 2.1 µM, and 5.1 µM without LiCl, i.e. on average 3.4 ± 1.6 µM, and 2.1 µM, 0.9 µM, and 0.8 µM with LiCl present, i.e. on average 1.3 ± 0.8 µM. The obtained values are in line with earlier fluorescence measurements of the Cu^{2+} binding affinity to the $A\beta_{40}$ peptide, although this affinity is known to vary with the pH, the buffer, and other experimental conditions (Ghalebani *et al.*, 2012; Alies *et al.*, 2013). The difference between the average measured K_D values is not significant at the 5% level with a two-tailed t-test, which shows that Li^+ ions are not able to compete with Cu^{2+} for binding to Aβ. Thus, the Li^+ binding affinity for $A\beta_{40}$ is likely in the millimolar range, or weaker.

CD spectroscopy: effects of Li^+ ions on $A\beta_{40}$ structure in SDS

Although Aβ peptides are generally disordered in aqueous solutions, they adopt an α-helical secondary structure in membranes and membrane-mimicking environments such as SDS micelles (Tiiman *et al.*, 2016; Österlund *et al.*, 2018). Thus, the CD spectrum for $A\beta_{40}$ in sodium phosphate buffer displays the characteristic minimum for random coil structure at 198 nm (Fig. 6). Addition of 50 mM SDS, which is well above the critical concentration for micelle formation (Österlund *et al.*, 2018), induces an alpha-helical structure with characteristic minima around 208 and 222 nm. Titrating LiCl in concentrations up to 512 µM to the $A\beta_{40}$ sample slightly increases the general CD intensity, but does not change the overall spectral shape – the minima remain at their respective positions. The intensity changes are not caused by dilution of the sample during the titration, as the added volumes are very small, and as dilution would not increase but rather decrease the CD intensity. The observed changes in CD intensity therefore suggest a small but distinct binding effect of LiCl ions. This binding effect appears to be much weaker than the structural rearrangements and Aβ coil-coil-interactions previously reported to be induced by Cu^{2+} ions (Tiiman *et al.*, 2016).

BN-PAGE: effects of Li^+ ions on $A\beta_{42}$ oligomer formation and stability

Well-defined and SDS-stabilized $A\beta_{42}$ oligomers were prepared in the presence of different amounts of LiCl. SDS treatment of $A\beta_{42}$ peptides at low concentrations ($\leq$ 7 mM) leads to formation of stable and homogeneous $A\beta_{42}$ oligomers of certain sizes and conformations (Barghorn *et al.*, 2005; Rangachari *et al.*, 2007). As shown in Fig. 7, two sizes of $A\beta_{42}$ oligomers are formed in presence of the two SDS concentrations. In 0.2% (6.9 mM) SDS, small oligomers with a molecular weight (MW) around 16-20 kDa are formed. These oligomers appear to contain a large fraction of tetramers (Vosough & Barth, manuscript). In

0.05% (1.7 mM) SDS, larger oligomers with MWs around 55-60 kD are formed (Barghorn *et al.*, 2005). These larger oligomers, which most likely contain twelve $A\beta_{42}$ monomers, display a globular morphology and are therefore sometimes called globulomers (Barghorn *et al.*, 2005).

All oligomers were analyzed by BN-PAGE instead of by SDS-PAGE to avoid disruption of the non-cross linked $A\beta_{42}$ oligomers by the high (>1%) SDS concentrations used in SDS-PAGE (Bitan *et al.*, 2005). As shown in lanes 2-5 and 6-9 of Fig. 7, increasing LiCl concentrations have weak or no effects on the size or homogeneity of the formed $A\beta_{42}$ oligomers, as the bands retain their shape and intensity. Only for the globulomers subjected to the highest LiCl concentration (10 mM) is the intensity of the BN-PAGE band slightly reduced (lane 5, Fig 7).

FTIR spectroscopy: effects of Li^+ ions on $A\beta_{42}$ oligomer structure

The secondary structures of $A\beta_{42}$ oligomers formed with different Li^+ concentrations were studied with FTIR spectroscopy, where the amide I region (1700-1600 cm^{-1}) is very sensitive to changes in the protein backbone conformation. The technique is useful also in amyloid research, given its capacity to characterize β-sheets (Barth, 2007; Sarroukh *et al.*, 2013).

Fig. 8 shows second derivative IR spectra for the amide I region of $A\beta_{42}$ globulomers (Fig. 8A) and smaller oligomers (Fig. 8B), prepared with different concentrations of Li^+ ions. Monomeric $A\beta_{42}$ displayed a relatively broad band at 1639-1640 cm^{-1}, which is in agreement with the position of the band for disordered (random coil) polypeptides measured in D_2O (Barth, 2007). For both types of $A\beta_{42}$ oligomers, this main band is much narrower and downshifted by about 10 cm^{-1}, while a second smaller band appears around 1685 cm^{-1}. This split band pattern is indicative of an anti-parallel β-sheet conformation (Cerf *et al.*, 2009).

Earlier studies in our laboratory have shown a relationship between the position and width of this main band, and the size and homogeneity of the $A\beta_{42}$ oligomers (Vosough & Barth, manuscript). The lower band position of the larger oligomers is in line with this relationship and our previous results, and confirms the different sizes of the oligomers produced at the two SDS concentrations. We have recently observed that a number of transition metal ions induce significant effects on the main band position for $A\beta_{42}$ oligomers (manuscript in preparation). Because the spectra for $A\beta_{42}$ oligomers formed with different amounts of LiCl generally superimpose on the IR spectra for the Li^+-free oligomers, with no shifts observed for the main band, it appears that Li^+ ions have no significant effect on the oligomers' size or secondary structure.

DISCUSSION

Lithium as a therapeutic agent

Lithium has no known biological functions in the human body. Li^+ ions readily pass biological membranes, and are evenly distributed in tissues and easily eliminated via the kidneys (Nordberg *et al.*, 2015). Li^+ ions are however far from inert, and several well-defined medical conditions related to abnormal Li^+ concentrations exist. In low blood concentrations, Li^+ is used as a medication for bipolar and schizoaffective disorders (Machado-Vieira *et al.*, 2009), but at higher concentrations Li^+ ions are neurotoxic (Sellers *et al.*, 1982; Emilien & Maloteaux, 1996; Nordberg *et al.*, 2015; Wen *et al.*, 2019). This leaves a narrow therapeutic window of 0.6 -1.2 mM that has to be closely monitored in order to prevent Li^+ intoxication, which is easily recognized by EEG (Mignarri *et al.*, 2013) and treatable by reducing the therapeutic dose. Li^+ intoxication (>1.5 mM) presents as apathy, vertigo, tremor and gastrointestinal symptoms, in more severe cases confusion, psychosis, myoclonus and cardiac

arrhythmias (Nordberg *et al.*, 2015). Li^+ intoxication affects also the kidneys with polyuria and elevated U-albumin although overt renal failure is rare (Nordberg *et al.*, 2015).

Treatment of bipolar and schizoaffective disorders with Li^+ has generated some knowledge about Li^+ metabolism in the human body (Wen *et al.*, 2019; Medic *et al.*, 2020). Li^+ accumulates to some extent in bone (Birch, 1974), and chronic Li^+ effects are implicated in osteomalacia and severe osteoporosis (Roos, 2014). Patients treated with Li^+ also show an increased frequency of hypothyroidism and goitre, and widespread effects on several facets of the endocrine system have been noted (Salata & Klein, 1987). The negative effects of Li^+ on thyroid function have been clearly demonstrated in a study on populations in the Andean Mountains, where natural exposure to Li^+ is high, and where urinary Li^+ was found to correlate negatively with free thyroxine (T_4) but correlate positively with the pituitary gland hormone thyrotropin (Broberg *et al.*, 2011). The toxicity of Li^+ is further emphasized by studies from regions with naturally elevated concentrations of Li^+ in potable water, where reduced fetal size has been noted to correlate linearly with increases in blood Li^+ (Harari *et al.*, 2015).

To what extent Li^+ treatment reduces the development of AD symptoms is unclear (Engel *et al.*, 2008; Mauer *et al.*, 2014; Nordberg *et al.*, 2015; Sutherland & Duthie, 2015). Bipolar disorder increases the risk of AD when compared to the general population, and Li^+ treatment seems to reduce this risk (Velosa *et al.*, 2020), but the mechanisms mediating this effect are far from elucidated (Kerr *et al.*, 2018). In rare cases even regular-dose long-time Li^+ therapy may cause severe intoxication of the central nervous system, characterized by cerebellar dysfunction and cognitive decline (Emilien & Maloteaux, 1996).

Lithium interactions with the $A\beta_{40}$ peptide

The NMR (Figs. 3 and 4), fluorescence quenching (Fig. 5), and CD (Fig. 6) experiments show that Li^+ ions display weak interaction with the $A\beta_{40}$ peptide, where the binding affinity for the $Li^+ \cdot A\beta_{40}$ complex may be in the millimolar range. The IR and CD results show minor or no effects of Li^+ ions on the secondary structures of $A\beta_{40}$ monomers (Fig. 6) and $A\beta_{42}$ oligomers (Fig. 8). The Li^+ ions may have a small effect on Aβ aggregation, with minor perturbations on the morphology of aggregated $A\beta_{40}$ fibrils (Fig. 2), and effects on the $A\beta_{40}$ aggregation kinetics (Fig. 1; Table 1) and $A\beta_{42}$ oligomer stability (Fig. 7) only at very high Li^+ concentrations. These results are in line with previous computer modeling results, which suggest small differences between how the monovalent K^+, Li^+, and Na^+ alkali ions affect Aβ oligomerization (Huraskin & Horn, 2019).

As $A\beta_{40}$ and $A\beta_{42}$ have identical N-terminal sequences, the two peptide variants should interact very similarly with Li^+ ions, which were found to bind to the N-terminal Aβ region (Fig. 3B). The weak affinity between $A\beta_{40}$ and Li^+ ions, and the fact that Li^+ does not efficiently compete with Cu^{2+} ions for Aβ binding (Fig. 4), suggest that Li^+ ions are not coordinated by specific binding ligands. Instead, Li^+ likely engages in non-specific electrostatic interactions with the negatively charged Aβ residues, i.e. D1, E3, D7, E11, E22, and D23 (which are located in the N-terminal and central regions).

The weak binding affinity to $A\beta_{40}$ peptides is not caused by Li^+ ions being monovalent, as e.g. monovalent Ag^+ ions display rather strong and specific binding to Aβ peptides (Wallin *et al.*, 2020). Moreover, divalent Pb^{2+} and trivalent Cr^{3+} ions do not bind strongly to Aβ, while divalent Cu^{2+}, Mn^{2+} and Zn^{2+} as well as tetravalent Pb^{4+} ions do (Faller, 2009; Abelein *et al.*, 2015; Tiiman *et al.*, 2016; Wallin *et al.*, 2016; Wallin *et al.*, 2017). Thus, Aβ/metal interactions are not governed by the charge of the metal ion, but rather by its specific properties, such as ionic radius and electron configuration ($1s^2$ for Li^+).

It is illustrative to compare the Aβ interactions with Li^+ ions to the well-studied interactions with Cu^{2+} and Zn^{2+} ions. These two divalent ions display residue-specific interactions with Aβ peptides, displaying binding affinities in the micromolar-nanomolar range and strong effects on Aβ secondary structure, aggregation, and diffusion (Danielsson *et al.*, 2007; Faller, 2009; Lindgren *et al.*, 2013; Abelein *et al.*, 2015; Tiiman *et al.*, 2016; Owen *et al.*, 2019). Aβ binding to Cu^{2+} and Zn^{2+} is coordinated mainly by residue-specific interactions with the N-terminal His residues, i.e. H6, H13, and H14 (Faller, 2009; Lindgren *et al.*, 2013; Abelein *et al.*, 2015; Tiiman *et al.*, 2016). The biological relevance of Cu^{2+} and Zn^{2+} ions in AD pathology is demonstrated by their dysregulation in AD patients (Wang *et al.*, 2015; Szabo *et al.*, 2016), and by them being accumulated in plaques of Aβ aggregates in AD brains (Beauchemin & Kisilevsky, 1998; Lovell *et al.*, 1998; Miller *et al.*, 2006). During neuronal signaling Cu^{2+} and Zn^{2+} ions are released into the synaptic clefts (Ayton *et al.*, 2013), where they may interact with Aβ peptides to initiate Aβ aggregation (Branch *et al.*, 2017), or modulate the formation and toxicity of Aβ oligomers (Stefaniak & Bal, 2019; Wärmländer *et al.*, 2019).

The current results indicate that Li^+ ions are not able to compete with Cu^{2+} or Zn^{2+} ions for binding to Aβ peptides, and should therefore not be able to influence the *in vivo* effects of Cu^{2+} and Zn^{2+} ions on Aβ aggregation and toxicity. Although high concentrations of Li^+ showed some effects on Aβ aggregation (Figs. 1-3;7), these effects are likely at least partly related to ionic strength effects (Abelein *et al.*, 2016). Under physiological ionic strength, no specific interactions are observed between $Aβ_{40}$ monomers and Li^+ ions (Fig. 3C,D). Thus, we conclude that the previously reported possible beneficial effects of Li^+ on Alzheimer's disease progression (Mauer *et al.*, 2014; Sutherland & Duthie, 2015; Kerr *et al.*, 2018; Hampel *et al.*, 2019; Velosa *et al.*, 2020) seem not to be caused by direct interactions between Li^+ ions and Aβ peptides.

ACKNOWLEDGMENTS: We thank Elizabeth (Li) Wang for helpful discussions. This work was supported by grants from the Swedish Alzheimer Foundation and the Swedish Research Council to AG, the Swedish Brain Foundation to AG and AB, the Magnus Bergvall Foundation to SW and PR, the Ulla-Carin Lindquist ALS Foundation to PR, and from Olle Engkvist's Foundation, the Stockholm Region, and Knut and Alice Wallenberg Foundation to AB.

CONFICT OF INTEREST: The authors declare no conflict of interest.

REFERENCES

Abelein A, Abrahams JP, Danielsson J, Gräslund A, Jarvet J, Luo J, Tiiman A, Wärmländer SK (2014). The hairpin conformation of the amyloid beta peptide is an important structural motif along the aggregation pathway. *J Biol Inorg Chem* **19**(4-5): 623-634. doi: 10.1007/s00775-014-1131-8.

Abelein A, Gräslund A, Danielsson J (2015). Zinc as chaperone-mimicking agent for retardation of amyloid beta peptide fibril formation. *Proc Natl Acad Sci U S A* **112**(17): 5407-5412. doi: 10.1073/pnas.1421961112.

Abelein A, Jarvet J, Barth A, Gräslund A, Danielsson J (2016). Ionic Strength Modulation of the Free Energy Landscape of Abeta40 Peptide Fibril Formation. *J Am Chem Soc* **138**(21): 6893-6902. doi: 10.1021/jacs.6b04511.

Adlard PA, Bush AI (2018). Metals and Alzheimer's Disease: How Far Have We Come in the Clinic? *J Alzheimers Dis* **62**(3): 1369-1379. doi: 10.3233/JAD-170662.

Agostinho P, Cunha RA, Oliveira C (2010). Neuroinflammation, oxidative stress and the pathogenesis of Alzheimer's disease. *Curr Pharm Des* **16**(25): 2766-2778. doi: 10.2174/138161210793176572.

Al-Hilaly YK, Williams TL, Stewart-Parker M, Ford L, Skaria E, Cole M, Bucher WG, Morris KL, Sada AA, Thorpe JR, Serpell LC (2013). A central role for dityrosine crosslinking of Amyloid-beta in Alzheimer's disease. *Acta Neuropathol Commun* **1**: 83. doi: 10.1186/2051-5960-1-83.

Alies B, Renaglia E, Rozga M, Bal W, Faller P, Hureau C (2013). Cu(II) affinity for the Alzheimer's peptide: tyrosine fluorescence studies revisited. *Anal Chem* **85**(3): 1501-1508. doi: 10.1021/ac302629u.

Ayton S, Lei P, Bush AI (2013). Metallostasis in Alzheimer's disease. *Free Radic Biol Med* **62**: 76-89. doi: 10.1016/j.freeradbiomed.2012.10.558.

Baldassarre M, Barth A (2014). Pushing the detection limit of infrared spectroscopy for structural analysis of dilute protein samples. *Analyst* **139**(21): 5393-5399. doi: 10.1039/c4an00918e.

Barghorn S, Nimmrich V, Striebinger A, Krantz C, P K, Janson B, Bahr M, Schmidt M, Bitner RS, Harlan J, Barlow E, Ebert U, Hillen H (2005). Globular amyloid β-peptide1-42 oligomer – a homogenous and stable neuropathological protein in Alzheimer's disease. *J Neurochem* **95**: 834–847.

Baronio CM, Baldassarre M, Barth A (2019). Insight into the internal structure of amyloid-beta oligomers by isotope-edited Fourier transform infrared spectroscopy. *Phys Chem Chem Phys* **21**(16): 8587-8597. doi: 10.1039/c9cp00717b.

Barth A (2007). Infrared spectroscopy of proteins. *Biochim Biophys Acta* **1767**(9): 1073-1101. doi: 10.1016/j.bbabio.2007.06.004.

Beauchemin D, Kisilevsky R (1998). A method based on ICP-MS for the analysis of Alzheimer's amyloid plaques. *Anal Chem* **70**(5): 1026-1029.

Birch NJ (1974). Lithium accumulation in bone after oral administration in rat and in man. *Clin Sci Mol Med* **46**(3): 409-413. doi: 10.1042/cs0460409.

Bitan G, Fradinger EA, Spring SM, Teplow DB (2005). Neurotoxic protein oligomers--what you see is not always what you get. *Amyloid* **12**(2): 88-95. doi: 10.1080/13506120500106958.

Branch T, Barahona M, Dodson CA, Ying L (2017). Kinetic Analysis Reveals the Identity of Abeta-Metal Complex Responsible for the Initial Aggregation of Abeta in the Synapse. *ACS Chem Neurosci* **8**(9): 1970-1979. doi: 10.1021/acschemneuro.7b00121.

Broberg K, Concha G, Engstrom K, Lindvall M, Grander M, Vahter M (2011). Lithium in drinking water and thyroid function. *Environ Health Perspect* **119**(6): 827-830. doi: 10.1289/ehp.1002678.

Budni J, Feijo DP, Batista-Silva H, Garcez ML, Mina F, Belletini-Santos T, Krasilchik LR, Luz AP, Schiavo GL, Quevedo J (2017). Lithium and memantine improve spatial memory impairment and neuroinflammation induced by beta-amyloid 1-42 oligomers in rats. *Neurobiol Learn Mem* **141**: 84-92. doi: 10.1016/j.nlm.2017.03.017.

Caccamo A, Oddo S, Tran LX, LaFerla FM (2007). Lithium reduces tau phosphorylation but not A beta or working memory deficits in a transgenic model with both plaques and tangles. *Am J Pathol* **170**(5): 1669-1675. doi: 10.2353/ajpath.2007.061178.

Cardillo GM, De-Paula VJR, Ikenaga EH, Costa LR, Catanozi S, Schaeffer EL, Gattaz WF, Kerr DS, Forlenza OV (2018). Chronic Lithium Treatment Increases Telomere Length in Parietal Cortex and Hippocampus of Triple-Transgenic Alzheimer's Disease Mice. *J Alzheimers Dis* **63**(1): 93-101. doi: 10.3233/JAD-170838.

Cerf E, Sarroukh R, Tamamizu-Kato S, Breydo L, Derclaye S, Dufrene YF, Narayanaswami V, Goormaghtigh E, Ruysschaert JM, Raussens V (2009). Antiparallel beta-sheet: a signature structure of the oligomeric amyloid beta-peptide. *Biochem J* **421**(3): 415-423. doi: 10.1042/BJ20090379.

Chin-Chan M, Navarro-Yepes J, Quintanilla-Vega B (2015). Environmental pollutants as risk factors for neurodegenerative disorders: Alzheimer and Parkinson diseases. *Front Cell Neurosci* **9**: 124. doi: 10.3389/fncel.2015.00124.

Cho CH, Urquidi J, Singh S, Wilse Robinson G (1999). Thermal Offset Viscosities of Liquid H2O, D2O, and T2O. *J. Phys. Chem. B* **103**(11): 1991-1994.

Danielsson J, Andersson A, Jarvet J, Gräslund A (2006). 15N relaxation study of the amyloid beta-peptide: structural propensities and persistence length. *Magn Reson Chem* **44 Spec No**: S114-121. doi: 10.1002/mrc.1814.

Danielsson J, Jarvet J, Damberg P, Gräslund A (2002). Translational diffusion measured by PFG-NMR on full length and fragments of the Alzheimer Aβ(1–40) peptide. Determination of hydrodynamic radii of random coil peptides of varying length. *Magnetic Resonance in Chemistry* **40**(13): S89-S97.

Danielsson J, Pierattelli R, Banci L, Gräslund A (2007). High-resolution NMR studies of the zinc-binding site of the Alzheimer's amyloid beta-peptide. *FEBS J* **274**(1): 46-59. doi: 10.1111/j.1742-4658.2006.05563.x.

Decker M, Munoz-Torrero D (2016). Special Issue: "Molecules against Alzheimer". *Molecules* **21**(12) doi: 10.3390/molecules21121736.

Dell'Osso L, Del Grande C, Gesi C, Carmassi C, Musetti L (2016). A new look at an old drug: neuroprotective effects and therapeutic potentials of lithium salts. *Neuropsychiatr Dis Treat* **12**: 1687-1703. doi: 10.2147/NDT.S106479.

Donix M, Bauer M (2016). Population Studies of Association Between Lithium and Risk of Neurodegenerative Disorders. *Curr Alzheimer Res* **13**(8): 873-878. doi: 10.2174/1567205013666160219112957.

Duce JA, Bush AI, Adlard PA (2011). Role of amyloid-β–metal interactions in Alzheimer's disease. *Future Neurol* **6**(5): 641–659.

Edelhoch H (1967). Spectroscopic Determination of Tryptophan and Tyrosine in Proteins. *Biochemistry* **6**(7): 1948–1954.

Emilien G, Maloteaux JM (1996). Lithium neurotoxicity at low therapeutic doses Hypotheses for causes and mechanism of action following a retrospective analysis of published case reports. *Acta Neurol Belg* **96**(4): 281-293.

Engel T, Goni-Oliver P, Gomez de Barreda E, Lucas JJ, Hernandez F, Avila J (2008). Lithium, a potential protective drug in Alzheimer's disease. *Neurodegener Dis* **5**(3-4): 247-249. doi: 10.1159/000113715.

Faller P (2009). Copper and zinc binding to amyloid-beta: coordination, dynamics, aggregation, reactivity and metal-ion transfer. *Chembiochem* **10**(18): 2837-2845. doi: 10.1002/cbic.200900321.

Forlenza OV, De-Paula VJ, Diniz BS (2014). Neuroprotective effects of lithium: implications for the treatment of Alzheimer's disease and related neurodegenerative disorders. *ACS Chem Neurosci* **5**(6): 443-450. doi: 10.1021/cn5000309.

Fornai F, Longone P, Cafaro L, Kastsiuchenka O, Ferrucci M, Manca ML, Lazzeri G, Spalloni A, Bellio N, Lenzi P, Modugno N, Siciliano G, Isidoro C, Murri L, Ruggieri S, Paparelli A (2008). Lithium delays progression of amyotrophic lateral sclerosis. *Proc Natl Acad Sci U S A* **105**(6): 2052-2057. doi: 10.1073/pnas.0708022105.

Frozza RL, Lourenco MV, De Felice FG (2018). Challenges for Alzheimer's Disease Therapy: Insights from Novel Mechanisms Beyond Memory Defects. *Front Neurosci* **12**: 37. doi: 10.3389/fnins.2018.00037.

Gade Malmos K, Blancas-Mejia LM, Weber B, Buchner J, Ramirez-Alvarado M, Naiki H, Otzen D (2017). ThT 101: a primer on the use of thioflavin T to investigate amyloid formation. *Amyloid* **24**(1): 1-16. doi: 10.1080/13506129.2017.1304905.

Ge W, Jakobsson E (2018). Systems Biology Understanding of the Effects of Lithium on Affective and Neurodegenerative Disorders. *Front Neurosci* **12**: 933. doi: 10.3389/fnins.2018.00933.

Ghalebani L, Wahlström A, Danielsson J, Wärmländer SK, Gräslund A (2012). pH-dependence of the specific binding of Cu(II) and Zn(II) ions to the amyloid-beta peptide. *Biochem Biophys Res Commun* **421**(3): 554-560. doi: 10.1016/j.bbrc.2012.04.043.

Gibbons GS, Lee VMY, Trojanowski JQ (2019). Mechanisms of Cell-to-Cell Transmission of Pathological Tau: A Review. *JAMA Neurol* **76**(1): 101-108. doi: 10.1001/jamaneurol.2018.2505.

Glasoe PK, Long FA (1960). Use of glass electrodes to measure acidities in deuterium oxide. *J Phys Chem* **64**: 88–90.

Glenner GG, Wong CW (1984). Alzheimer's disease: initial report of the purification and characterization of a novel cerebrovascular amyloid protein. *Biochem Biophys Res Commun* **120**(3): 885-890.

Goedert M (2018). Tau filaments in neurodegenerative diseases. *FEBS Lett* **592**(14): 2383-2391. doi: 10.1002/1873-3468.13108.

Habib A, Sawmiller D, Li S, Xiang Y, Rongo D, Tian J, Hou H, Zeng J, Smith A, Fan S, Giunta B, Mori T, Currier G, Shytle DR, Tan J (2017). LISPRO mitigates beta-amyloid and associated pathologies in Alzheimer's mice. *Cell Death Dis* **8**(6): e2880. doi: 10.1038/cddis.2017.279.

Habib A, Shytle RD, Sawmiller D, Koilraj S, Munna SA, Rongo D, Hou H, Borlongan CV, Currier G, Tan J (2019). Comparing the effect of the novel ionic cocrystal of lithium salicylate proline (LISPRO) with lithium carbonate and lithium salicylate on memory and behavior in female APPswe/PS1dE9 Alzheimer's mice. *J Neurosci Res* **97**(9): 1066-1080. doi: 10.1002/jnr.24438.

Hampel H, Lista S, Mango D, Nistico R, Perry G, Avila J, Hernandez F, Geerts H, Vergallo A, Alzheimer Precision Medicine I (2019). Lithium as a Treatment for Alzheimer's Disease: The Systems Pharmacology Perspective. *J Alzheimers Dis* **69**(3): 615-629. doi: 10.3233/JAD-190197.

Harari F, Langeen M, Casimiro E, Bottai M, Palm B, Nordqvist H, Vahter M (2015). Environmental exposure to lithium during pregnancy and fetal size: a longitudinal study in the Argentinean Andes. *Environ Int* **77**: 48-54. doi: 10.1016/j.envint.2015.01.011.

Heppner FL, Ransohoff RM, Becher B (2015). Immune attack: the role of inflammation in Alzheimer disease. *Nat Rev Neurosci* **16**(6): 358-372. doi: 10.1038/nrn3880.

Huat TJ, Camats-Perna J, Newcombe EA, Valmas N, Kitazawa M, Medeiros R (2019). Metal Toxicity Links to Alzheimer's Disease and Neuroinflammation. *J Mol Biol* **431**(9): 1843-1868. doi: 10.1016/j.jmb.2019.01.018.

Huraskin D, Horn AHC (2019). Alkali ion influence on structure and stability of fibrillar amyloid-beta oligomers. *J Mol Model* **25**(2): 37. doi: 10.1007/s00894-018-3920-4.

Kerr F, Bjedov I, Sofola-Adesakin O (2018). Molecular Mechanisms of Lithium Action: Switching the Light on Multiple Targets for Dementia Using Animal Models. *Front Mol Neurosci* **11**: 297. doi: 10.3389/fnmol.2018.00297.

Kisby B, Jarrell JT, Agar ME, Cohen DS, Rosin ER, Cahill CM, Rogers JT, Huang X (2019). Alzheimer's Disease and Its Potential Alternative Therapeutics. *J Alzheimers Dis Parkinsonism* **9**(5) doi: 10.4172/2161-0460.1000477.

Lee SJ, Nam E, Lee HJ, Savelieff MG, Lim MH (2017). Towards an understanding of amyloid-beta oligomers: characterization, toxicity mechanisms, and inhibitors. *Chem Soc Rev* **46**(2): 310-323. doi: 10.1039/c6cs00731g.

Lindgren J, Segerfeldt P, Sholts SB, Gräslund A, Karlström AE, Wärmländer SK (2013). Engineered non-fluorescent Affibody molecules facilitate studies of the amyloid-beta (Abeta) peptide in monomeric form: low pH was found to reduce Abeta/Cu(II) binding affinity. *J Inorg Biochem* **120**: 18-23. doi: 10.1016/j.jinorgbio.2012.11.005.

Liu M, Qian T, Zhou W, Tao X, Sang S, Zhao L (2020). Beneficial effects of low-dose lithium on cognitive ability and pathological alteration of Alzheimer's disease transgenic mice model. *Neuroreport* **31**(13): 943-951. doi: 10.1097/WNR.0000000000001499.

Lovell MA, Robertson JD, Teesdale WJ, Campbell JL, Markesbery WR (1998). Copper, iron and zinc in Alzheimer's disease senile plaques. *J Neurol Sci* **158**(1): 47-52.

Luo J, Mohammed I, Wärmländer SK, Hiruma Y, Gräslund A, Abrahams JP (2014). Endogenous polyamines reduce the toxicity of soluble abeta peptide aggregates associated with Alzheimer's disease. *Biomacromolecules* **15**(6): 1985-1991. doi: 10.1021/bm401874j.

Luo J, Otero JM, Yu CH, Wärmländer SK, Gräslund A, Overhand M, Abrahams JP (2013). Inhibiting and reversing amyloid-beta peptide (1-40) fibril formation with gramicidin S and engineered analogues. *Chemistry* **19**(51): 17338-17348. doi: 10.1002/chem.201301535.

Luo J, Wärmländer SK, Gräslund A, Abrahams JP (2014). Alzheimer peptides aggregate into transient nanoglobules that nucleate fibrils. *Biochemistry* **53**(40): 6302-6308. doi: 10.1021/bi5003579.

Luo J, Wärmländer SK, Gräslund A, Abrahams JP (2016). Cross-interactions between the Alzheimer Disease Amyloid-beta Peptide and Other Amyloid Proteins: A Further Aspect of the Amyloid Cascade Hypothesis. *J Biol Chem* **291**(32): 16485-16493. doi: 10.1074/jbc.R116.714576.

Luo J, Yu CH, Yu H, Borstnar R, Kamerlin SC, Gräslund A, Abrahams JP, Wärmländer SK (2013). Cellular polyamines promote amyloid-beta (Abeta) peptide fibrillation and modulate the aggregation pathways. *ACS Chem Neurosci* **4**(3): 454-462. doi: 10.1021/cn300170x.

Machado-Vieira R, Manji HK, Zarate CA, Jr. (2009). The role of lithium in the treatment of bipolar disorder: convergent evidence for neurotrophic effects as a unifying hypothesis. *Bipolar Disord* **11 Suppl 2**: 92-109. doi: 10.1111/j.1399-5618.2009.00714.x.

Mauer S, Vergne D, Ghaemi SN (2014). Standard and trace-dose lithium: a systematic review of dementia prevention and other behavioral benefits. *Aust N Z J Psychiatry* **48**(9): 809-818. doi: 10.1177/0004867414536932.

Medic B, Stojanovic M, Stimec BV, Divac N, Vujovic KS, Stojanovic R, Colovic M, Krstic D, Prostran M (2020). Lithium - Pharmacological and Toxicological Aspects: The Current State of the Art. *Curr Med Chem* **27**(3): 337-351. doi: 10.2174/0929867325666180904124733.

Mignarri A, Chini E, Rufa A, Rocchi R, Federico A, Dotti MT (2013). Lithium neurotoxicity mimicking rapidly progressive dementia. *J Neurol* **260**(4): 1152-1154. doi: 10.1007/s00415-012-6820-z.

Miller LM, Wang Q, Telivala TP, Smith RJ, Lanzirotti A, Miklossy J (2006). Synchrotron-based infrared and X-ray imaging shows focalized accumulation of Cu and Zn co-localized with beta-amyloid deposits in Alzheimer's disease. *J Struct Biol* **155**(1): 30-37. doi: 10.1016/j.jsb.2005.09.004.

Mital M, Wezynfeld NE, Fraczyk T, Wiloch MZ, Wawrzyniak UE, Bonna A, Tumpach C, Barnham KJ, Haigh CL, Bal W, Drew SC (2015). A Functional Role for Abeta in Metal Homeostasis? N-Truncation and High-Affinity Copper Binding. *Angew Chem Int Ed Engl* **54**(36): 10460-10464. doi: 10.1002/anie.201502644.

Modgil S, Lahiri DK, Sharma VL, Anand A (2014). Role of early life exposure and environment on neurodegeneration: implications on brain disorders. *Transl Neurodegener* **3**: 9. doi: 10.1186/2047-9158-3-9.

Morris G, Berk M (2016). The Putative Use of Lithium in Alzheimer's Disease. *Curr Alzheimer Res* **13**(8): 853-861. doi: 10.2174/1567205013666160219113112.

Morrison KE, Dhariwal S, Hornabrook R, Savage L, Burn DJ, Khoo TK, Kelly J, Murphy CL, Al-Chalabi A, Dougherty A, Leigh PN, Wijesekera L, Thornhill M, Ellis CM, O'Hanlon K, Panicker J, Pate L, Ray P, Wyatt L, Young CA, Copeland L, Ealing J, Hamdalla H, Leroi I, Murphy C, O'Keeffe F, Oughton E, Partington L, Paterson P, Rog D, Sathish A, Sexton D, Smith J, Vanek H, Dodds S, Williams TL, Steen IN, Clarke J, Eziefula C, Howard R, Orrell R, Sidle K, Sylvester R, Barrett W, Merritt C, Talbot K, Turner MR, Whatley C, Williams C, Williams J, Cosby C, Hanemann CO, Iman I, Philips C, Timings L, Crawford SE, Hewamadduma C, Hibberd R, Hollinger H, McDermott C, Mils G, Rafiq M, Shaw PJ, Taylor A, Waines E, Walsh T, Addison-Jones R, Birt J, Hare M, Majid T (2013). Lithium in patients with amyotrophic lateral sclerosis (LiCALS): a phase 3 multicentre, randomised, double-blind, placebo-controlled trial. *Lancet Neurol* **12**(4): 339-345. doi: 10.1016/S1474-4422(13)70037-1.

Nath S, Agholme L, Kurudenkandy FR, Granseth B, Marcusson J, Hallbeck M (2012). Spreading of neurodegenerative pathology via neuron-to-neuron transmission of beta-amyloid. *J Neurosci* **32**(26): 8767-8777. doi: 10.1523/JNEUROSCI.0615-12.2012.

Nečas D, Klapetek P (2012). Gwyddion: an open-source software for SPM data analysis. *Central European Journal of Physics* **10**: 181-188. doi: https://doi.org/10.2478.

Nery LR, Eltz NS, Hackman C, Fonseca R, Altenhofen S, Guerra HN, Freitas VM, Bonan CD, Vianna MR (2014). Brain intraventricular injection of amyloid-beta in zebrafish embryo impairs cognition and increases tau phosphorylation, effects reversed by lithium. *PLoS One* **9**(9): e105862. doi: 10.1371/journal.pone.0105862.

Nordberg G, Fowler B, Nordberg M, (eds). (2015). Handbook on the Toxicology of Metals, Elsevier.

Owen MC, Gnutt D, Gao M, Wärmländer SKTS, Jarvet J, Gräslund A, Winter R, Ebbinghaus S, Strodel B (2019). Effects of in vivo conditions on amyloid aggregation. *Chem Soc Rev* **48**(14): 3946-3996. doi: 10.1039/c8cs00034d.

Pan Y, Short JL, Newman SA, Choy KHC, Tiwari D, Yap C, Senyschyn D, Banks WA, Nicolazzo JA (2018). Cognitive benefits of lithium chloride in APP/PS1 mice are associated with enhanced brain clearance of beta-amyloid. *Brain Behav Immun* **70**: 36-47. doi: 10.1016/j.bbi.2018.03.007.

Priebe GA, Kanzawa MM (2020). Reducing the progression of Alzheimer's disease in Down syndrome patients with micro-dose lithium. *Med Hypotheses* **137**: 109573. doi: 10.1016/j.mehy.2020.109573.

Prince M, Wimo A, Guerchet M, Ali G-C, Wu Y-T, Prina M (2015). World Alzheimer Report 2015 - The Global Impact of Dementia. London, UK.

Querfurth HW, LaFerla FM (2010). Alzheimer's disease. *N Engl J Med* **362**(4): 329-344. doi: 10.1056/NEJMra0909142.

Rangachari V, Moore BD, Reed DK, Sonoda LK, Bridges AW, Conboy E, Hartigan D, Rosenberry TL (2007). Amyloid-beta(1-42) rapidly forms protofibrils and oligomers by distinct pathways in low concentrations of sodium dodecylsulfate. *Biochemistry* **46**(43): 12451-12462. doi: 10.1021/bi701213s.

Regen F, Hellmann-Regen J, Costantini E, Reale M (2017). Neuroinflammation and Alzheimer's Disease: Implications for Microglial Activation. *Curr Alzheimer Res* **14**(11): 1140-1148. doi: 10.2174/1567205014666170203141717.

Rocha NKR, Themoteo R, Brentani H, Forlenza OV, De Paula VJR (2020). Neuronal-Glial Interaction in a Triple-Transgenic Mouse Model of Alzheimer's Disease: Gene Ontology and Lithium Pathways. *Front Neurosci* **14**: 579984. doi: 10.3389/fnins.2020.579984.

Rockenstein E, Torrance M, Adame A, Mante M, Bar-on P, Rose JB, Crews L, Masliah E (2007). Neuroprotective effects of regulators of the glycogen synthase kinase-3beta signaling pathway in a transgenic model of Alzheimer's disease are associated with reduced amyloid precursor protein phosphorylation. *J Neurosci* **27**(8): 1981-1991. doi: 10.1523/JNEUROSCI.4321-06.2007.

Roos PM (2014). Osteoporosis in neurodegeneration. *J Trace Elem Med Biol* **28**(4): 418-421. doi: 10.1016/j.jtemb.2014.08.010.

Ryves WJ, Harwood AJ (2001). Lithium inhibits glycogen synthase kinase-3 by competition for magnesium. *Biochem Biophys Res Commun* **280**(3): 720-725. doi: 10.1006/bbrc.2000.4169.

Salata R, Klein I (1987). Effects of lithium on the endocrine system: a review. *J Lab Clin Med* **110**(2): 130-136.

Sardar Sinha M, Ansell-Schultz A, Civitelli L, Hildesjo C, Larsson M, Lannfelt L, Ingelsson M, Hallbeck M (2018). Alzheimer's disease pathology propagation by exosomes containing toxic amyloid-beta oligomers. *Acta Neuropathol* **136**(1): 41-56. doi: 10.1007/s00401-018-1868-1.

Sarroukh R, Goormaghtigh E, Ruysschaert JM, Raussens V (2013). ATR-FTIR: a "rejuvenated" tool to investigate amyloid proteins. *Biochim Biophys Acta* **1828**(10): 2328-2338. doi: 10.1016/j.bbamem.2013.04.012.

Selkoe DJ, Hardy J (2016). The amyloid hypothesis of Alzheimer's disease at 25 years. *EMBO Mol Med* **8**(6): 595-608. doi: 10.15252/emmm.201606210.

Sellers J, Tyrer P, Whiteley A, Banks DC, Barer DH (1982). Neurotoxic effects of lithium with delayed rise in serum lithium levels. *Br J Psychiatry* **140**: 623-625. doi: 10.1192/bjp.140.6.623.

Sengupta U, Nilson AN, Kayed R (2016). The Role of Amyloid-beta Oligomers in Toxicity, Propagation, and Immunotherapy. *EBioMedicine* **6**: 42-49. doi: 10.1016/j.ebiom.2016.03.035.

Sofola-Adesakin O, Castillo-Quan JI, Rallis C, Tain LS, Bjedov I, Rogers I, Li L, Martinez P, Khericha M, Cabecinha M, Bahler J, Partridge L (2014). Lithium suppresses Abeta pathology by inhibiting translation in an adult Drosophila model of Alzheimer's disease. *Front Aging Neurosci* **6**: 190. doi: 10.3389/fnagi.2014.00190.

Stefaniak E, Bal W (2019). Cu(II) Binding Properties of N-Truncated Abeta Peptides: In Search of Biological Function. *Inorg Chem* **58**(20): 13561-13577. doi: 10.1021/acs.inorgchem.9b01399.

Sutherland C, Duthie AC (2015). Invited commentary on ... Lithium treatment and risk for dementia in adults with bipolar disorder. *Br J Psychiatry* **207**(1): 52-54. doi: 10.1192/bjp.bp.114.161729.

Szabo ST, Harry GJ, Hayden KM, Szabo DT, Birnbaum L (2016). Comparison of Metal Levels between Postmortem Brain and Ventricular Fluid in Alzheimer's Disease and Nondemented Elderly Controls. *Toxicol Sci* **150**(2): 292-300. doi: 10.1093/toxsci/kfv325.

Tiiman A, Luo J, Wallin C, Olsson L, Lindgren J, Jarvet J, Roos PM, Sholts SB, Rahimipour S, Abrahams JP, Karlström AE, Gräslund A, Wärmländer SKTS (2016). Specific Binding of Cu(II) Ions to Amyloid-Beta Peptides Bound to Aggregation-Inhibiting Molecules or SDS Micelles Creates Complexes that Generate Radical Oxygen Species. *J Alzheimers Dis* **54**(3): 971-982. doi: 10.3233/JAD-160427.

Trujillo-Estrada L, Jimenez S, De Castro V, Torres M, Baglietto-Vargas D, Moreno-Gonzalez I, Navarro V, Sanchez-Varo R, Sanchez-Mejias E, Davila JC, Vizuete M, Gutierrez A, Vitorica J (2013). In vivo modification of Abeta plaque toxicity as a novel neuroprotective lithium-mediated therapy for Alzheimer's disease pathology. *Acta Neuropathol Commun* **1**: 73. doi: 10.1186/2051-5960-1-73.

Velosa J, Delgado A, Finger E, Berk M, Kapczinski F, de Azevedo Cardoso T (2020). Risk of dementia in bipolar disorder and the interplay of lithium: a systematic review and meta-analyses. *Acta Psychiatr Scand* doi: 10.1111/acps.13153.

Vosough F, Barth A (manuscript). Characterization of homogeneous and heterogeneous amyloid-β42 oligomer preparations with biochemical methods and infrared spectroscopy reveals a correlation between infrared spectrum and oligomer size.

Wallin C, Friedemann M, Sholts SB, Noormagi A, Svantesson T, Jarvet J, Roos PM, Palumaa P, Gräslund A, Wärmländer SKTS (2020). Mercury and Alzheimer's Disease: Hg(II) Ions Display Specific Binding to the Amyloid-beta Peptide and Hinder Its Fibrillization. *Biomolecules* **10**(1): 44. doi: 10.3390/biom10010044.

Wallin C, Jarvet J, Biverstål H, Wärmländer S, Danielsson J, Gräslund A, Abelein A (2020). Metal ion coordination delays amyloid-beta peptide self-assembly by forming an aggregation-inert complex. *J Biol Chem* **295**(21): 7224-7234. doi: 10.1074/jbc.RA120.012738.

Wallin C, Kulkarni YS, Abelein A, Jarvet J, Liao Q, Strodel B, Olsson L, Luo J, Abrahams JP, Sholts SB, Roos PM, Kamerlin SC, Gräslund A, Wärmländer SK (2016). Characterization of Mn(II) ion binding to the amyloid-beta peptide in Alzheimer's disease. *J Trace Elem Med Biol* **38**: 183-193. doi: 10.1016/j.jtemb.2016.03.009.

Wallin C, Sholts SB, Österlund N, Luo J, Jarvet J, Roos PM, Ilag L, Gräslund A, Wärmländer S (2017). Alzheimer's disease and cigarette smoke components: effects of nicotine, PAHs, and Cd(II), Cr(III), Pb(II), Pb(IV) ions on amyloid-beta peptide aggregation. *Sci Rep* **7**(1): 14423. doi: 10.1038/s41598-017-13759-5.

Wang X, Wang W, Li L, Perry G, Lee HG, Zhu X (2014). Oxidative stress and mitochondrial dysfunction in Alzheimer's disease. *Biochim Biophys Acta* **1842**(8): 1240-1247. doi: 10.1016/j.bbadis.2013.10.015.

Wang ZX, Tan L, Wang HF, Ma J, Liu J, Tan MS, Sun JH, Zhu XC, Jiang T, Yu JT (2015). Serum Iron, Zinc, and Copper Levels in Patients with Alzheimer's Disease: A Replication Study and Meta-Analyses. *J Alzheimers Dis* **47**(3): 565-581. doi: 10.3233/JAD-143108.

Wen J, Sawmiller D, Wheeldon B, Tan J (2019). A Review for Lithium: Pharmacokinetics, Drug Design, and Toxicity. *CNS Neurol Disord Drug Targets* **18**(10): 769-778. doi: 10.2174/1871527318666191114095249.

Wilson EN, Do Carmo S, Welikovitch LA, Hall H, Aguilar LF, Foret MK, Iulita MF, Jia DT, Marks AR, Allard S, Emmerson JT, Ducatenzeiler A, Cuello AC (2020). NP03, a Microdose Lithium Formulation, Blunts Early Amyloid Post-Plaque Neuropathology in McGill-R-Thy1-APP Alzheimer-Like Transgenic Rats. *J Alzheimers Dis* **73**(2): 723-739. doi: 10.3233/JAD-190862.

Wärmländer S, Tiiman A, Abelein A, Luo J, Jarvet J, Söderberg KL, Danielsson J, Gräslund A (2013). Biophysical studies of the amyloid beta-peptide: interactions with metal ions and small molecules. *Chembiochem* **14**(14): 1692-1704. doi: 10.1002/cbic.201300262.

Wärmländer SKTS, Österlund N, Wallin C, Wu J, Luo J, Tiiman A, Jarvet J, Gräslund A (2019). Metal binding to the Amyloid-β peptides in the presence of biomembranes: potential mechanisms of cell toxicity. *Journal of Biological Inorganic Chemistry* **24**: 1189–1196

Xiang J, Cao K, Dong YT, Xu Y, Li Y, Song H, Zeng XX, Ran LY, Hong W, Guan ZZ (2020). Lithium chloride reduced the level of oxidative stress in brains and serums of APP/PS1 double transgenic mice via the regulation of GSK3beta/Nrf2/HO-1 pathway. *Int J Neurosci* **130**(6): 564-573. doi: 10.1080/00207454.2019.1688808.

Yu F, Zhang Y, Chuang DM (2012). Lithium reduces BACE1 overexpression, beta amyloid accumulation, and spatial learning deficits in mice with traumatic brain injury. *J Neurotrauma* **29**(13): 2342-2351. doi: 10.1089/neu.2012.2449.

Zhao L, Gong N, Liu M, Pan X, Sang S, Sun X, Yu Z, Fang Q, Zhao N, Fei G, Jin L, Zhong C, Xu T (2014). Beneficial synergistic effects of microdose lithium with pyrroloquinoline quinone in an Alzheimer's disease mouse model. *Neurobiol Aging* **35**(12): 2736-2745. doi: 10.1016/j.neurobiolaging.2014.06.003.

Österlund N, Kulkarni YS, Misiaszek AD, Wallin C, Krüger DM, Liao Q, Mashayekhy Rad F, Jarvet J, Strodel B, Wärmländer SKTS, Ilag LL, Kamerlin SCL, Gräslund A (2018). Amyloid-beta Peptide Interactions with Amphiphilic Surfactants: Electrostatic and Hydrophobic Effects. *ACS Chem Neurosci* **9**(7): 1680-1692. doi: 10.1021/acschemneuro.8b00065.

	20 μM $A\beta_{40}$	**1:1 Li^+:Aβ**	**10:1 Li^+:Aβ**	**100:1 Li^+:Aβ**
$t_{1/2}$ [hours]	3.7 ± 0.7	3.6 ± 2.1	3.8 ± 0.6	4.9 ± 1.3
r_{max} [$hours^{-1}$]	0.5 ± 0.1	0.4 ± 0.2	0.5 ± 0.2	0.4 ± 0.1

Table 1. Kinetic parameters for $A\beta_{40}$ fibril formation, i.e. aggregation half-time ($t_{1/2}$) and maximum aggregation rate (r_{max}), derived from fitting the curves in Fig. 1 to Eq. 1.

FIGURES

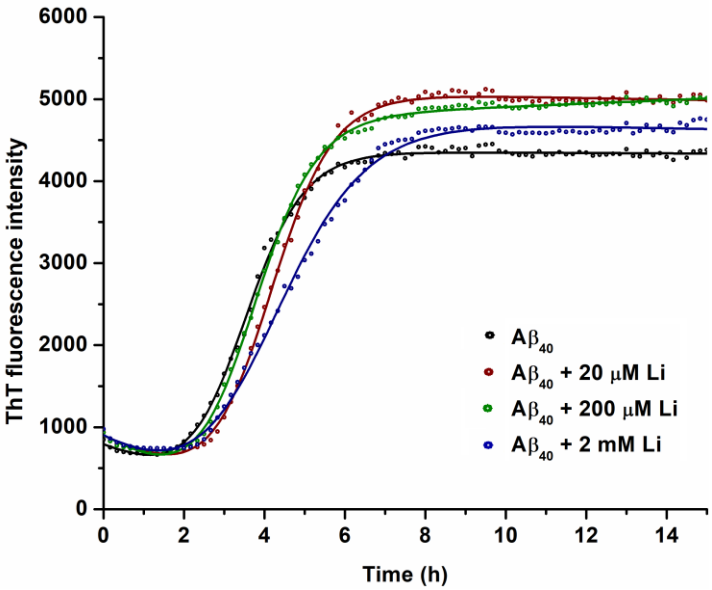

Fig. 1. Amyloid fibril formation monitored by ThT aggregation. Samples of 20 μM $A\beta_{40}$ peptides in 20 mM MES buffer, pH 7.35, were incubated at +37 °C together with 50 μM Thioflavin-T and different concentrations of LiCl: 0 μM – black; 20 μM – red; 200 μM – green; 2000 μM – blue. The circles represent average data points for four replicates, while the solid lines are derived from fitting to Eq. 1.

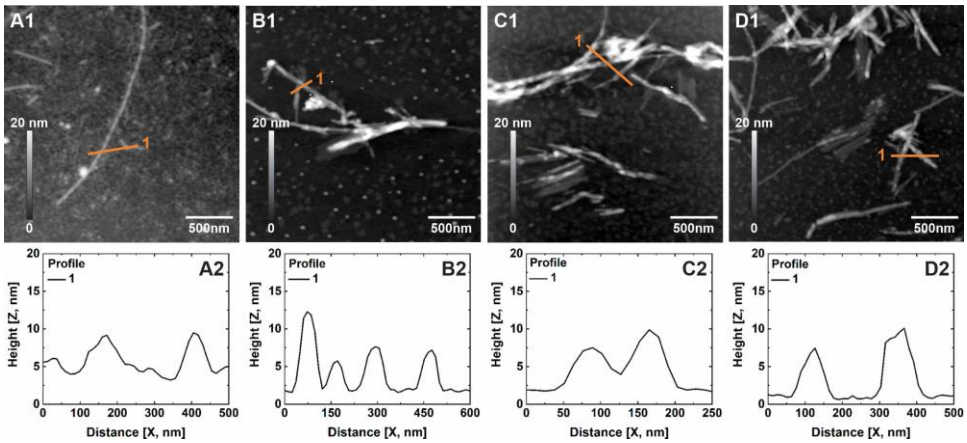

Fig. 2. Solid state AFM images (A1-D1) of aggregates of 20 μM $A\beta_{40}$, incubated in 5 mM MES buffer, pH 7.35, for 72 hours at +37 °C with 300 rpm shaking, together with different concentrations of LiCl. A. control sample - no LiCl; B. 20 μM LiCl; C. 200 μM LiCl; D. 2 mM LiCl. The height profile graphs (A2-D2) below the AFM images correspond to the cross-sections of $A\beta_{40}$ fibrils shown as white lines in the AFM images.

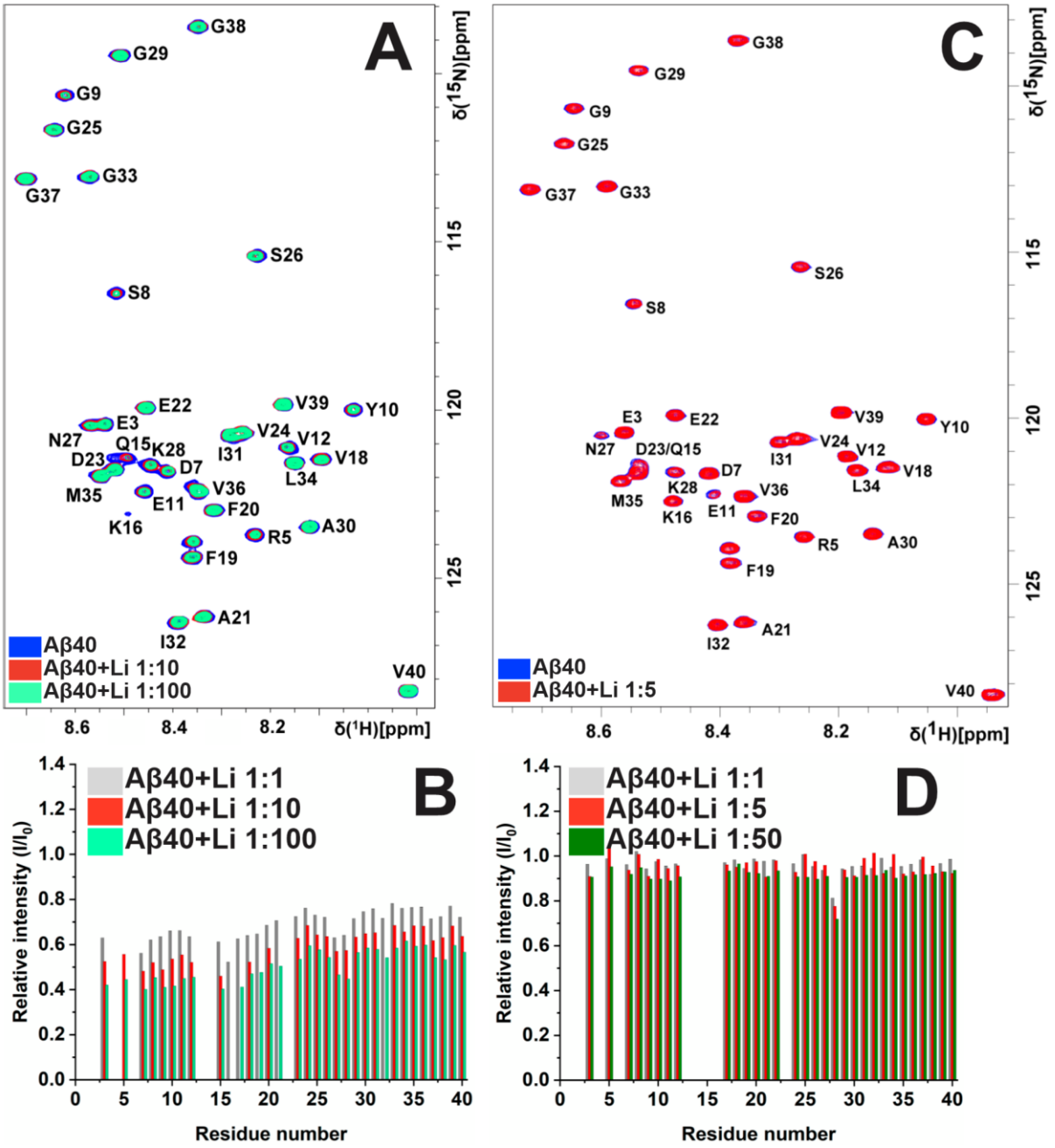

Fig. 3. NMR experiments for interactions between $A\beta_{40}$ monomers and Li^+ ions. (A) 2D ^1H-^{15}N-HSQC spectra of 92.4 μM ^{15}N-labeled $A\beta_{40}$ peptides in 20 mM MES buffer, pH 7.35 at +5 °C, recorded for $A\beta_{40}$ peptides alone (dark sky blue) and in the presence of either 924 μM LiCl (1:10 Aβ:Li ratio; passion red) or 9.24 mM LiCl (1:100 Aβ:Li ratio; Robin egg blue). (B) Relative intensities of $A\beta_{40}$ residue crosspeaks shown in (A), after addition of LiCl in 1:1, 1:10, and 1:100 Aβ:Li ratios. (C and D) similar experiments as in A and B, but carried out in the presence of 1x PBS buffer, and for Aβ:Li ratios of 1:1, 1:5, and 1:50.

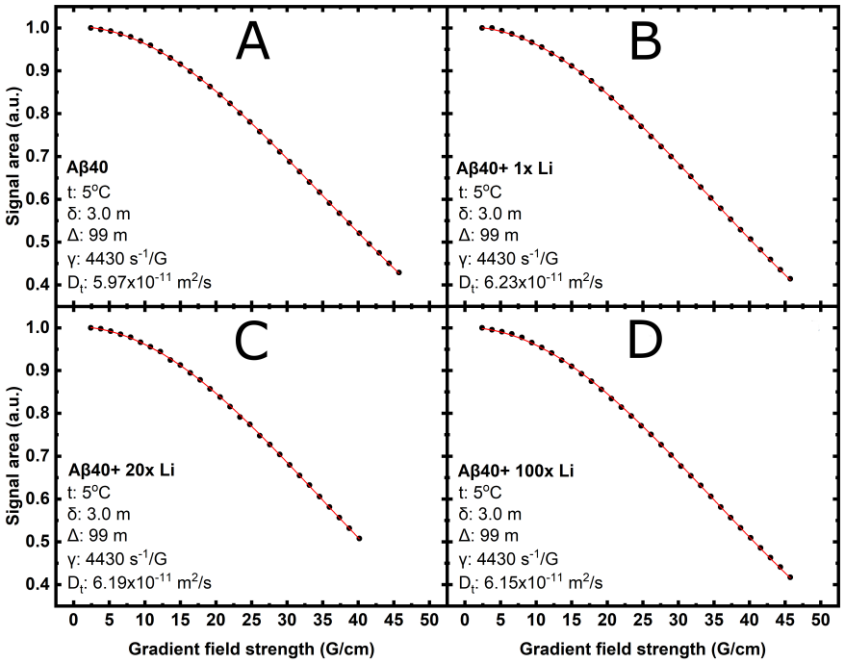

Fig. 4. NMR diffusion data for 55 μM $A\beta_{40}$ peptides in sodium phosphate buffer, pH 7.35 at +5 °C, recorded both in absence (A) and presence of different Li^+ concentrations, i.e. 55 μM (B), 1.1 mM (C), and 5.5 mM (D).

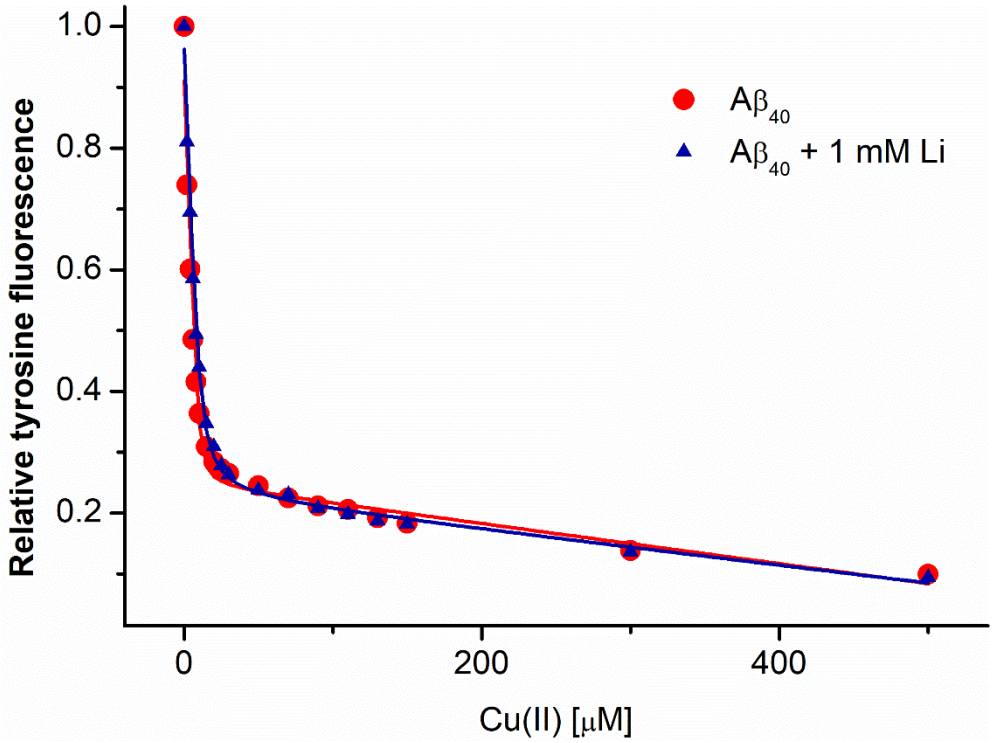

Fig. 5. Binding curves for the Cu^{2+}·$A\beta_{40}$ complex, obtained from the quenching effect of Cu^{2+} ions on the intrinsic fluorescence of Aβ residue Y10. $CuCl_2$ was titrated to 10 μM $A\beta_{40}$ in 20 mM MES buffer, pH 7.35 at 20 °C, both in the absence (red dots) and the presence (blue triangles) of 1 mM LiCl.

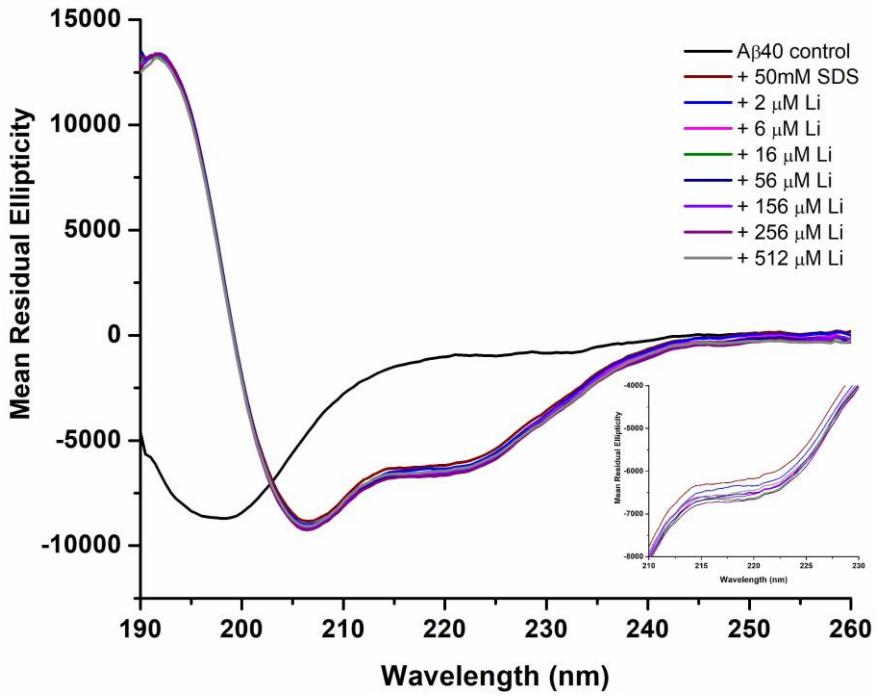

Fig. 6. CD spectra of 20 μM $A\beta_{40}$ peptides at 20 °C in 20 mM sodium phosphate buffer, pH 7.35. Spectra were recorded for Aβ in buffer only (black), after addition of 50 mM micellar SDS (brown), and after subsequent addition of between 2 μM (blue) and 512 μM (gray) of LiCl. The inset figure shows a close-up of the CD signals for the LiCl titration in the 210-230 nm range.

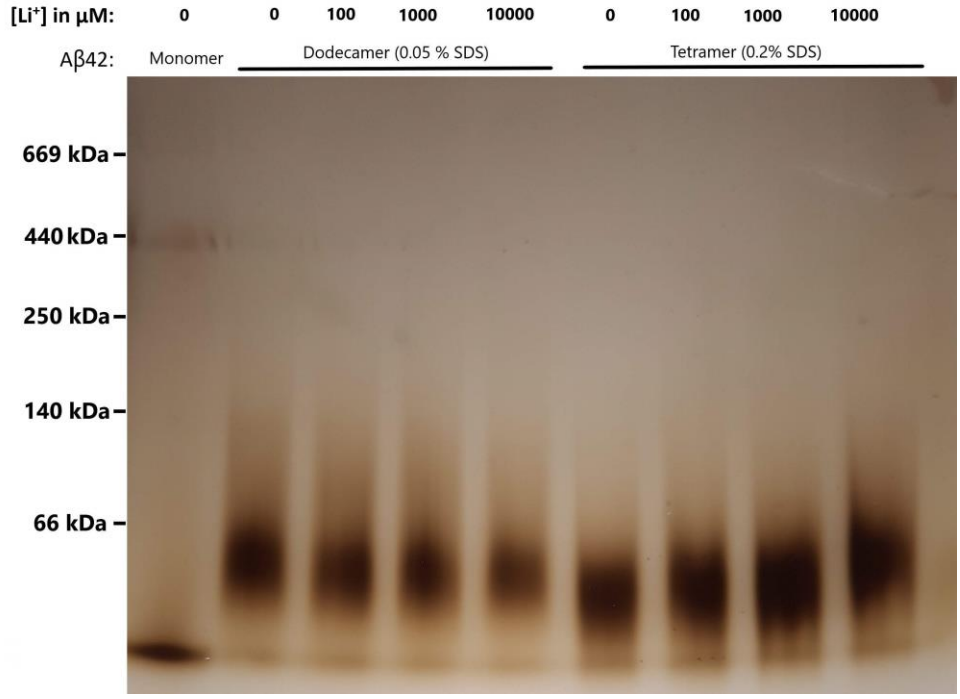

Fig. 7. BN-PAGE gel showing the effects of different concentrations of Li^+ ions on the formation of SDS-stabilized $A\beta_{42}$ oligomers. Lane 1: monomers prepared in 5 mM NaOD.

Lanes 2-5: $A\beta_{42}$ globulomers formed after 24 hours of incubation with 0.05% SDS and different LiCl concentrations. Lanes 6-9: $A\beta_{42}$ oligomers formed after 24 hours of incubation with 0.2% SDS and different LiCl concentrations.

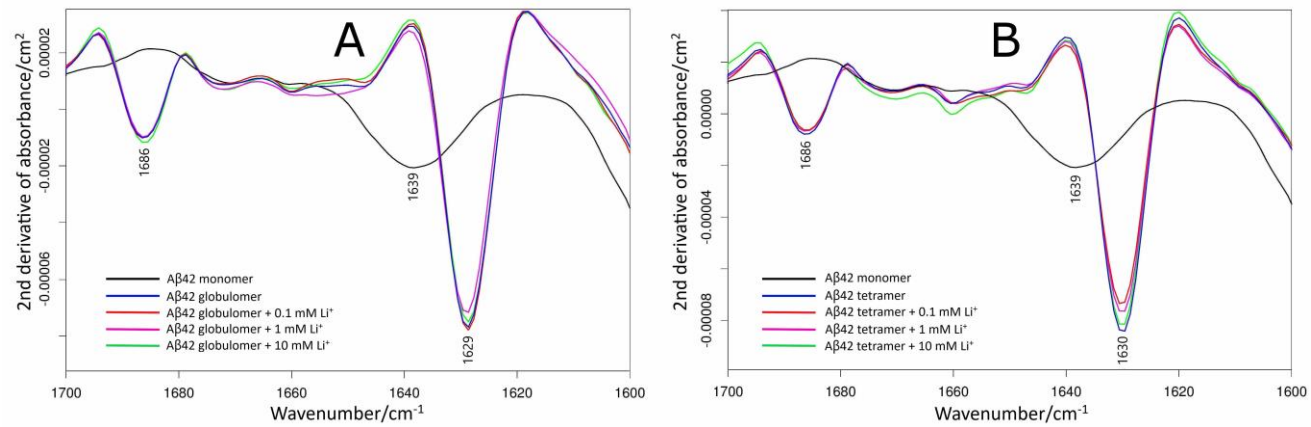

Fig. 8. Second derivatives of infrared absorbance spectra for 100 µM $A\beta_{42}$ monomers (black) and 80 µM SDS-stabilized $A\beta_{42}$ oligomers formed in absence (blue) and presence of 0.1 mM (red), 1 mM (purple), and 10 mM (green) of LiCl. The results are shown for $A\beta_{42}$ globulomers at 0.05% SDS (A) and smaller oligomers at 0.2% SDS (B).